Reductive Cleavage of Azoarene as a Key Step in Nickel-Catalyzed Amidation of Esters with Nitroarenes

Marten L. Ploeger,† Andrea Darù,‡ Jeremy N. Harvey,‡ and Xile Hu*,†*

†Laboratory of Inorganic Synthesis and Catalysis, Institute of Chemical Sciences and Engineering, École Polytechnique Fédérale de Lausanne (EPFL), ISIC-LSCI, BCH 3305, Lausanne 1015, Switzerland

‡Department of Chemistry, KU Leuven, Celestijnenlaan 200F, B-3001 Leuven, Belgium

ABSTRACT. A nickel-catalyzed reductive amidation of unactivated esters was recently reported, employing readily available and low-cost nitroarenes as nitrogen sources. Here we describe a comprehensive experimental and computational study, which reveals an intricate mechanism of this process. The reaction profile indicated azoarene as the terminal nitrogen intermediate formed from reduction of nitroarene. The activation of azoarene en route to amidation was probed by kinetics, Hammett plots, and DFT calculations. The activation likely involves Ni-catalyzed, $ZnCl_2$-promoted, reductive cleavage of the N=N double bond in an azoarene to form a bridging imido species, which then reacts in a rate-determining step with an ester to give an amide. Besides the nickel catalyst, $ZnCl_2$ has an important influence in the rates and orders of the reaction. DFT computations suggest $ZnCl_2$ stabilizes many of the intermediates in the reaction pathway of

azoarene activation, including forming the key Ni-Zn heterobimetallic imido intermediate. The mechanistic insights revealed in this study lay the foundation for the development of synthetic methods employing azoarenes as stable and easily accessible nitrogen sources.

Keywords: nickel catalysis; mechanism; azobenzene; amidation; kinetics

1. Introduction.

Nitroarenes are important synthetic intermediates for nitrogen-containing aromatic compounds.[1] They are readily available by nitration of parent arenes such as benzene, toluene, and xylene.[2] Until now, the dominating transformations of nitroarenes are reduction to anilines,[2] and to a less degree, nucleophilic replacement of the NO_2 groups.[3–7] Motivated by the wide availability and low cost nature of nitroarenes, a number of groups have started to develop synthetic methods exploiting other modes of transformation of nitroarenes.[8–13]

Our group have recently explored the coupling of nitroarenes with various electrophiles such as alkyl and aryl halides,[14,15] esters,[16] and amides[17] under reductive conditions. The reactions were typically conducted in the presence of a metal reductant such as Zn or Mn, and an oxygen-accepting Lewis acid such as trimethylsilylchloride (TMSCl). Preliminary mechanistic investigations indicated that the majority of these reactions did not proceed via anilines, the complete reduction products. Instead, species partially reduced from nitroarenes were directly converted into the final amines or amide products. Under reductive conditions, a nitroarene, e.g, nitrobenzene, may be converted to nitrosobenzene, phenylhydroxyamine, azoxybenzene, and azobenzene, among other intermediates (Scheme 1a).[18] Each of these species is a potential intermediate. Elucidating the role of a relevant intermediate and how it is transformed not only is important for understanding a particular transformation of nitroarenes, but may lead to a new general strategy in transforming nitroarenes.

Scheme 1. (A) A simplified reaction pathway for nitroarene reduction. (B) Our previously reported reductive amidation of esters with nitrobenzene

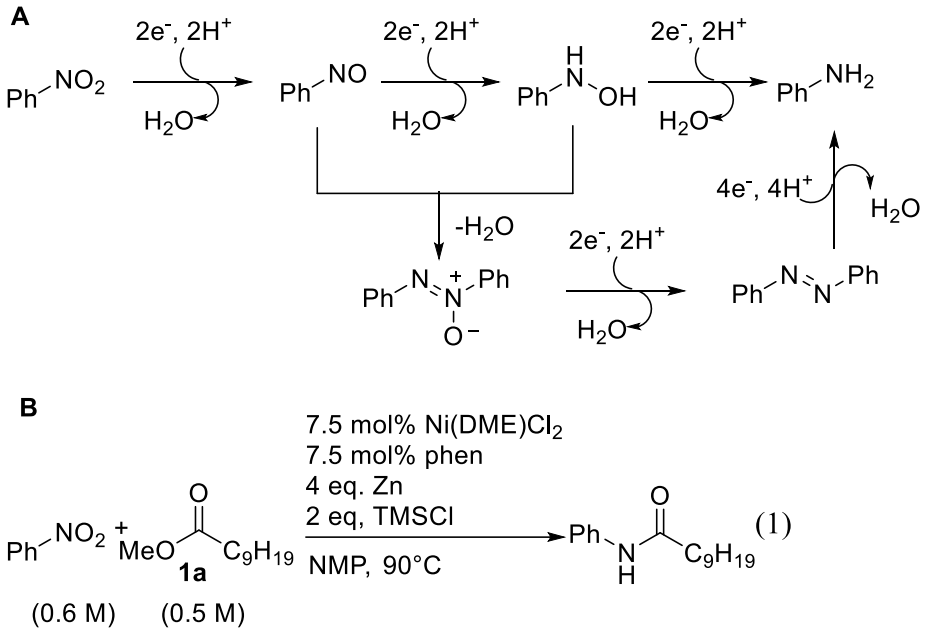

Here we describe a mechanistic study of Ni-catalyzed reductive amidation of non-activated esters with nitroarenes (Scheme 1B). While ester activation by oxidative addition to Ni is considered as a key step in a few Ni-catalyzed cross-coupling reactions of relatively activated esters (e.g., substituted by an aryl especially a naphthyl group),[19,20] preliminary study suggested such activation did not occur in our reaction.[16] Instead, a nitrogen species partially reduced from a nitroarene was activated by Ni before reacting with an ester to give the amide. The nitrogen species could be an arylhydroxylamine, nitrosoarene, azoxyarene, and azoarene, but not aniline. By following the reaction profile, we now confirm this nitrogen intermediate as azoarene. The mechanism of the coupling of an ester with an azoarene to give an amide under Ni catalysis is investigated by kinetic analysis, Hammett plots, as well as DFT computations. An unprecedented, Ni-catalyzed and $ZnCl_2$-promoted, reductive cleavage of azoarene is identified as a key step in the

amidation. This identification lays the foundation for the design of new synthetic methods harvesting the utility of azoarenes as readily available reagents.

2. Results

2.1. Identification of azoarene as the nitrogen intermediate

In a preliminary study, we tested various nitrogen species including phenylhydroxylamine, nitrosobenzene, azoxybenzene, azobenzene, and aniline as potential intermediates for the coupling of nitrobenzene with methyl decanoate (**1a**).[16] Phenylhydroxylamine, nitrosobenzene, azoxybenzene, and azobenzene, but not aniline, might replace nitrobenzene while maintaining a high yield of coupling. Azobenzene is the most reduced species among the four viable candidates, and it can be produced from the other three under reductive conditions, therefore it is thought to be the most likely downstream intermediate.

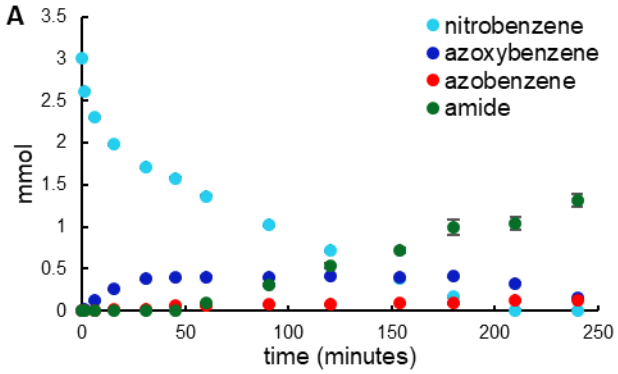

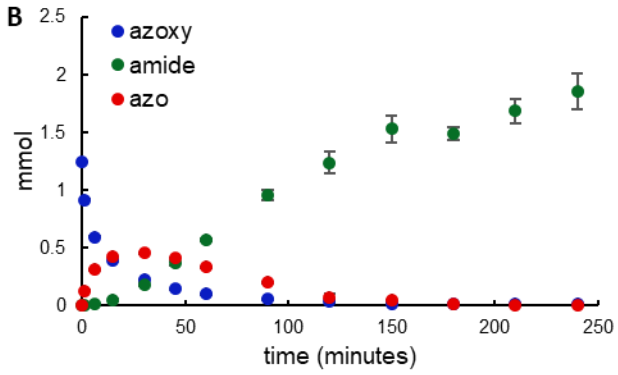

Figure 1. Reaction profiles of the amidation. (A) The evolution of the amount of different species present (in mmol) during the reductive amidation of **1a** with nitrobenzene. Conditions according to equation 1. (B) The evolution of the amount of different species present (in mmol) during the reductive amidation of **1a** with azoxybenzene. Conditions: 0.5 M 1a, 0.3 M azoxybenzene, 3 eq Zn, 0.5 eq TMSCl, 7.5 mol% $Ni(DME)Cl_2$, 7.5 mol% phenanthroline in 5 mL NMP at 90°C. For both graphs, sampling was performed in triplicate; the error bars indicate the sample standard error.

To probe this hypothesis, the reaction profile of the reductive amidation of **1a** with nitrobenzene was monitored by GC-MS (Figure 1A). The formation of amide was not observed until about a half of the nitrobenzene was converted. Among the possible intermediates (Scheme 1), only azoxybenzene and azobenzene were observed. Azoxybenzene was already formed at the beginning of the reaction and it reached a steady-state concentration before decaying at the end of the reaction. Azobenzene appeared after azoxybenzene, and its appearance coincided with the formation of amide. The reaction profile of the reductive amidation of **1a** with azoxybenzene was then monitored (Figure 1B). The conversion of azoxybenzene to azobenzene was quick, but the

formation of amide had a lag phase. The depletion of azobenzene coincided with the amide production. These results suggested that nitrobenzene was first converted to azobenzene under the reductive conditions, and azobenzene then reacted with an ester under Ni catalysis to give the amide.

2.2. Kinetics of Ni-catalyzed reductive coupling of azobenzene (2) with an ester (1a). As azobenzene was identified as the key nitrogen intermediate, the reaction of azobenzene and **1a** under relevant reductive coupling conditions (Figure 2A) was studied to elucidate the mechanism of the overall coupling. The kinetics of the reaction was monitored by *in situ* ATR-IR (Figure 2B and Figure S1, SI). As the reaction proceeded, signals of **1a** at 1145-1209 cm^{-1} and 1738 cm^{-1} decayed (labelled **1a** in Figure 2). Meanwhile, two peaks at 1055 cm^{-1} and 1537 cm^{-1} grew, which were tentatively attributed to the Zn-amide product (**P**), which was previously identified as the end product of amidation before quenching with a proton source in the workup.[16] As the reaction gave the amide product quantitatively with respect to **1a**, the conversion of **1a** reflected well the reaction progress. The concentrations of **1a** was estimated by the intensity of the IR peak at 1735 cm^{-1}.

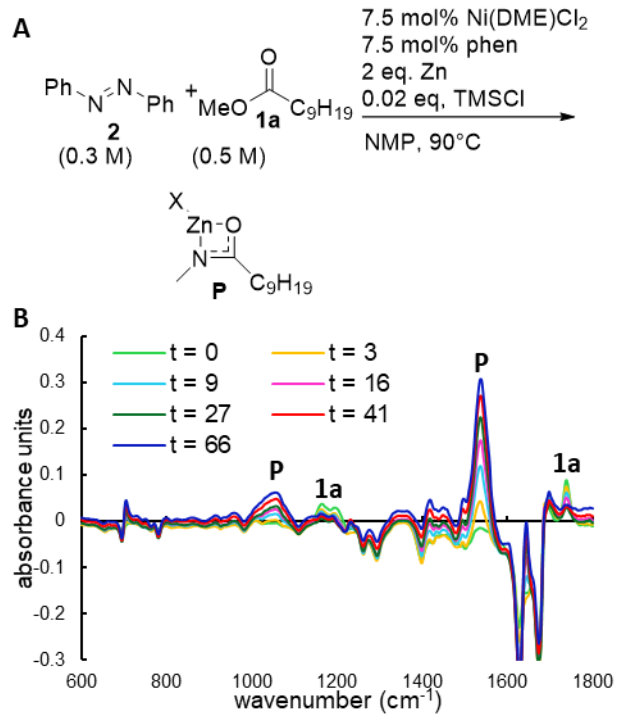

Figure 2. (A) Reaction scheme for Ni-catalyzed reductive coupling of azobenzene with **1a**. (B)Time-dependent IR spectra of the reaction mixture. The indicated times are in minutes. X = Cl or OMe.

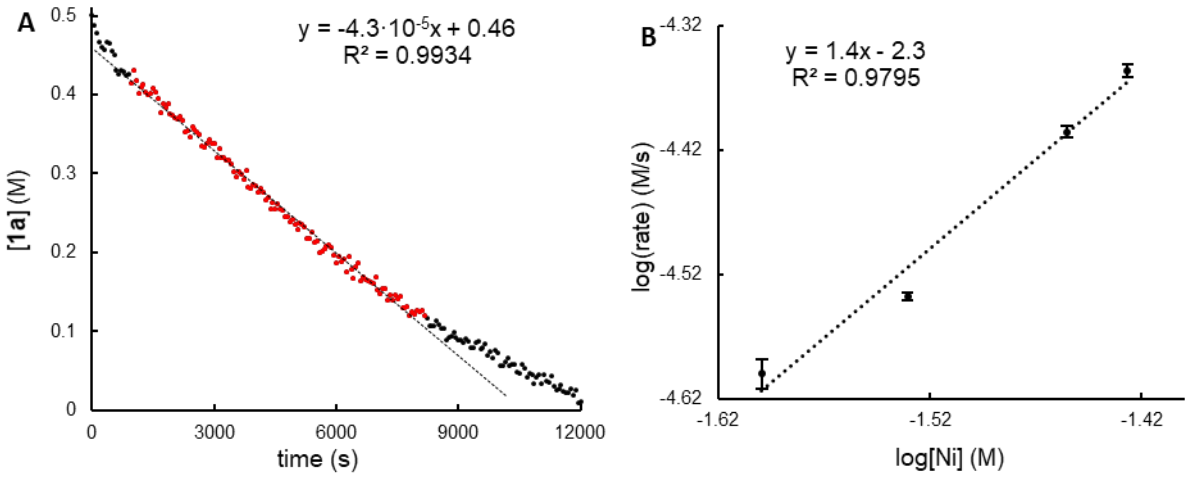

Figure 3. (A) A plot showing the decay of **1a** over the reaction time; conditions as in Fig. 2A; Red dots indicate the data used for the linear regression to determine the rate of the reaction. (B) log/log

plot of reaction rate versus the concentration of nickel catalyst. Values are averages over two runs. The error bars represent the standard error.

Under standard conditions (Figure 2A), **1a** underwent a linear decay (Figure 3A). This result indicated that the reaction was zero order in both **1a** and azobenzene under these conditions. The reactions were conducted under different loadings of catalysts (Fig. S2-S5, SI), and a log/log plot of the reaction rate versus catalyst concentration (Figure 3B) indicated an order of about 1.5 in Ni catalyst.

To probe whether the solid zinc particles influenced the rate determining step, the reaction rates were measured under different stirring rates (Figure S6, SI). The rates varied with the stirring rates, which suggested some involvement of heterogeneous Zn species in the rate determining step. Since $ZnCl_2$ was generated *in situ* from oxidation of Zn by a Ni species in this reaction, its influence was then probed by adding external $ZnCl_2$. An increase of the total concentration of $ZnCl_2$ (from both external and *in situ* sources) had two significant effects (Figure 4): (i) it accelerated the reaction; (ii) it changed the order of at least one of the substrates to non-zero so that the decay of **1a** was no longer linear when a significant amount of external $ZnCl_2$ was added. A saturation point was reached at a total $ZnCl_2$ concentration of 0.5M.

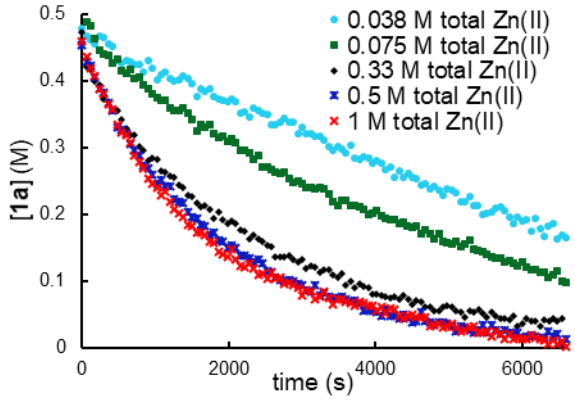

Figure 4. Influence of total $ZnCl_2$ concentration on the reaction rate. Conditions according to Figure 2A, with additional $ZnCl_2$ The total Zn(II) concentration is estimated from the sum of added $ZnCl_2$ and $Ni(DME)Cl_2$

The kinetics of the reaction were then measured at high total $ZnCl_2$ concentrations, and analyzed by Variable Time Normalization Analysis (VTNA) (Figure 5).[21,22] Two sets of experimental data were sufficient to deduce the reaction order by VTNA. The overlaying graphs indicated that the reaction was first order in Ni catalyst and zero order in azobenzene (Figure 5A-B). The reaction rates were the same under different stirring rates (Figure 5C), suggesting that only homogenous species were involved in the rate determining step when significant external $ZnCl_2$ was added. This result also suggested the stirring-rate dependence of the rates under no external $ZnCl_2$ addition was due to $ZnCl_2$ formation from heterogeneous Zn particles. To determine the order in ester, the initial amount of **1a** was varied. The concentration of azobenzene was estimated by deducing the reacted amount from the initial concentration assuming a perfect reaction stoichiometry. VTNA plot showed that the reaction was first order in **1a** (Figure 5D) at high total $ZnCl_2$ concentrations.

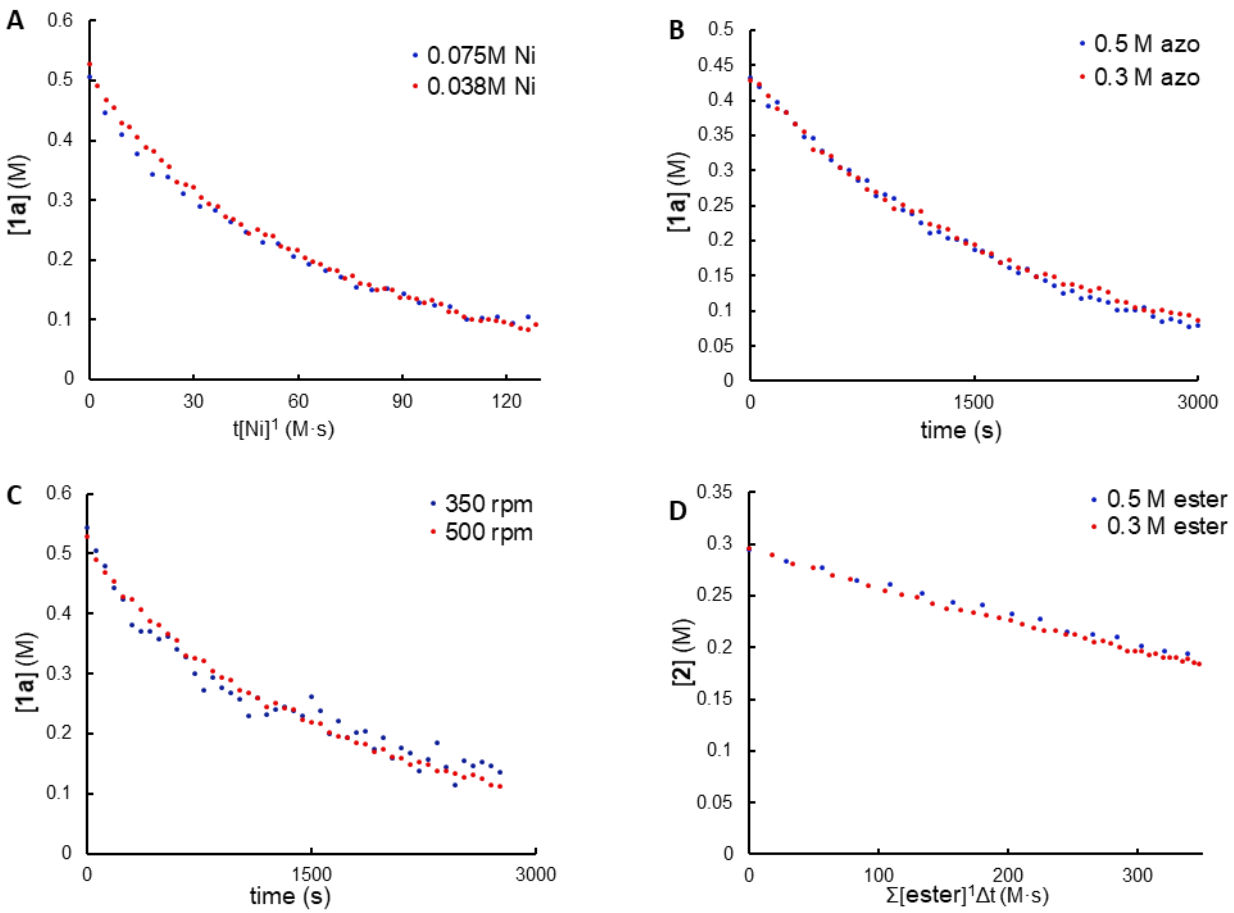

Figure 5. Kinetics at high total $ZnCl_2$ concentrations. General conditions: similar to Fig. 2A, but with additional $ZnCl_2$ to reach saturation with total Zn(II) concentration of 0.5 M. (A) Overlaying VTNA plots at two different concentrations of Ni catalyst. The X axis is *t*[Ni], where [Ni] is the total concentration of nickel, as determined by the weight of added $Ni(DME)Cl_2$. Overlap occurs only when the reaction is first order in nickel. (B) Overlaying VTNA plots at two different concentrations of **2** (azo). The X axis is time. Overlap occurs only if the reaction is zeroth order in **2**. (C) Overlaying reaction rate profiles at two different stirring rates. (D) Overlaying VTNA plots at different concentrations of **1a** (ester). The X axis is time multiplied by the approximate integral of [**1a**], where [**1a**] is the concentration of ester determined by FT-IR. Overlap occurs only if the reaction is first order in **1a**.

A competition experiment was conducted with and without external $ZnCl_2$ addition. An equal amount of **1a** and an aryl ester, methyl benzoate (**1b**), was treated with 1,2-bis(4-fluorophenyl)diazene (**2F**), producing a mixture of alkyl and aryl amides (Scheme 2 and Fig. S7, SI). Under standard conditions (shown in Fig. 2A), the ratio of alkyl to aryl amide was about 2.1:1. Addition of external $ZnCl_2$ (to reach saturation with a total concentration of 0.5 M) did not change the outcome of the coupling. This result suggests that addition of $ZnCl_2$ did not strongly change the nature of the active catalytic component of the system.[23]

Scheme 2. A competition experiment conducted with and without external $ZnCl_2$. Product ratios are averaged over two runs. Reported error is the standard error.

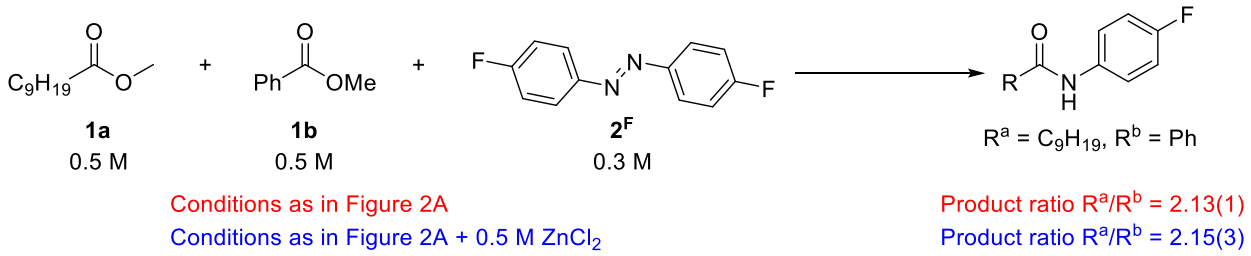

2.3. Hammett plots.

The rates of the reactions of **1a** with a series of azoarenes bearing different substituents at para-positions were measured at a high total $ZnCl_2$ concentration (Fig. S8-13, SI). A Hammett plot based on the observed rate constant is shown in Figure 6A. The reaction rate depends strongly on the nature of the para-substituent in a Volcano-like correlation. On the left side of the Volcano (NMe_2, OMe, and Me), the more electron-donating substituents slow down the reaction, but on the

right side (Me, F, H, and OCF_3), the more electron-withdrawing groups also slow down the reaction. This result suggests that two different rate laws or mechanisms apply: one for azoarenes with a strongly electron-donating group at the para-position, and the other one for other azoarenes (*i.e.* with Me, H, or electron-withdrawing para-substituents such as F and OCF_3). The majority of azoarenes substrates in the Ni-catalyzed reductive amidation belong to the latter category.

The relative reaction rate of azoarenes sitting at the right side of the Volcano plot in Figure 6A was then determined in a set of competition experiments. An equal amount of azobenzene and another azoarene was reacted with **1a** to give a mixture of amide products originating from two different azoarene partners. The ratio of the products correlates to the relative reaction rate (Figures S14-16, SI). A Hammett plot of the rate determined in this manner is shown in Figure 6B. In this case, a reverse trend was observed compared to Figure 6A, with the more electron-withdrawing substituent leading to a higher relative reaction rate.

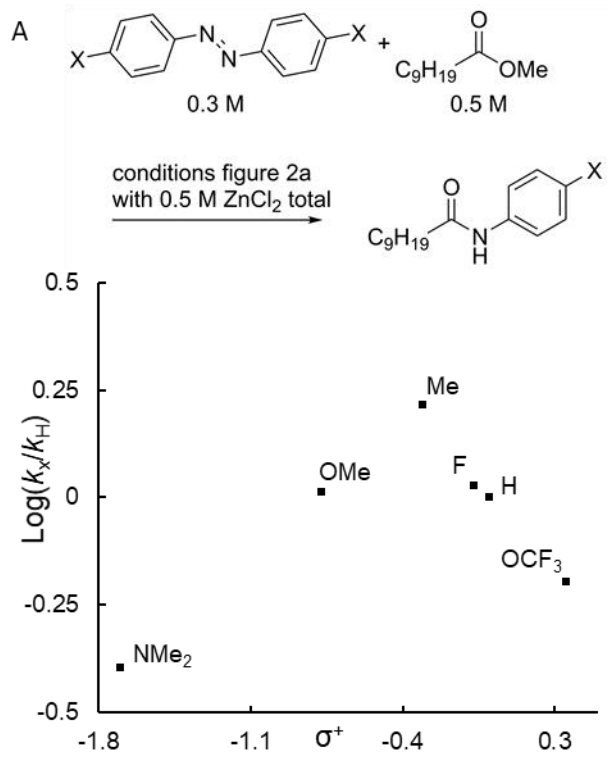

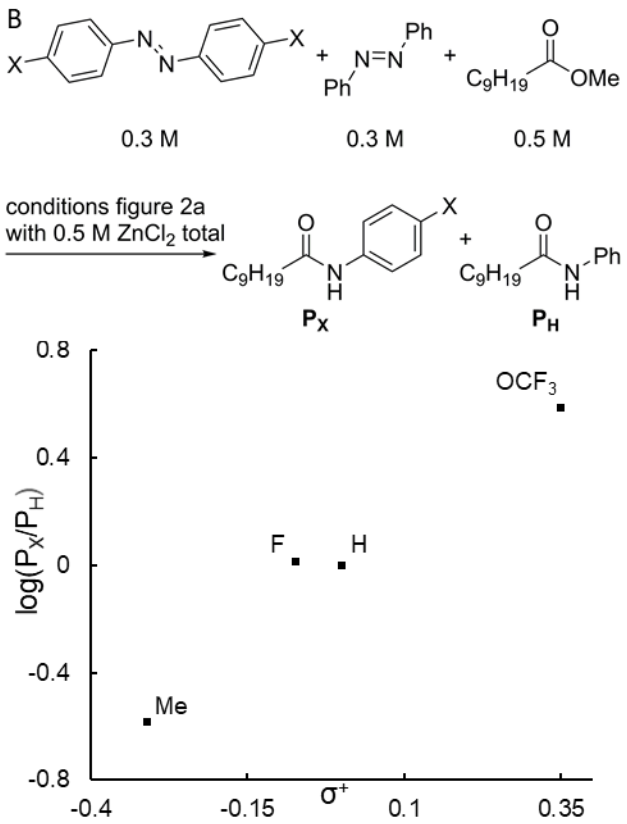

Figure 6. Hammett plots. (A) A plot using observed reaction rate constants; (B) A plot using relative reaction rate from competition experiments, determined by the product ratio at the end of the reaction. Conditions are similar to those in Figure 2A with additional $ZnCl_2$ to reach a total [Zn(II)] of 0.5 M.

2.4. Reactivity of Ni(0)-azoarene species. Given that the coupling is conducted under strongly reducing conditions in the presence of an excess amount of Zn, and an azoarene is the key downstream nitrogen intermediate, a Ni(0)-azoarene species is a likely Ni-bound intermediate. Several such species with varying supporting ligands were reported in the literature,[24–27] including one supported by a bipyridine ligand.[28] We tried to prepare an analogous species supported by phenanthroline (phen), the preferred ligand for the amidation, but our attempts were unsuccessful.

Recognizing that 2,2'-bipyridine (bipy) was also a viable ligand for the amidation with just a slightly lower yield than phen for a test reaction (94% versus 100%),[16] we decided to employ a [Ni(0)(azoarene)(bipy)] complex as the model intermediate. To enable product identification by ^{19}F NMR, we prepared the complex containing a para-F substituted azobenzene (**3F**). Under conditions mimicking those of the catalytic reaction (e.g., high [$ZnCl_2$]) but in absence of free azobenzene and solid zinc, the amidation product was obtained in 49% yield (based on Ni; Scheme 3), in addition to some free azoarene **2F** (34 %). Compound **3F** reacted with 1 equiv. of $ZnCl_2$ to give free azobenzene (ca. 50%) and other unidentified products (Fig. S20, SI). The reaction was faster with 13 equiv. of $ZnCl_2$ (Fig. S21, SI). The product mixture contained paramagnetic species as indicated by 1H NMR (Fig. S22, SI).

Scheme 3. Reaction of **3F** with **1a** under conditions mimicking the high-[$ZnCl_2$] catalytic reaction.

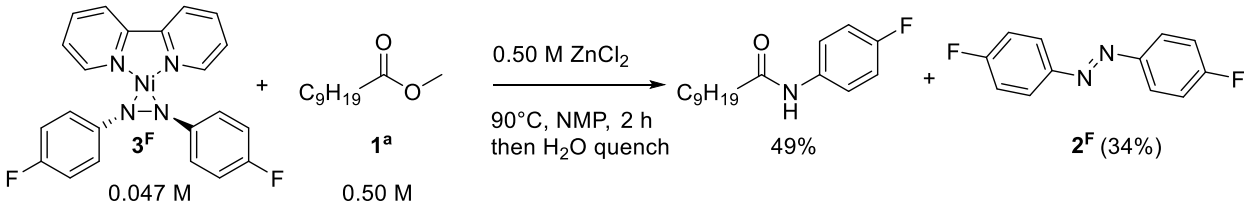

2.4 Computational study. We have performed density functional theory (DFT) computational studies in order to get insight into a possible mechanistic pathway. In brief, the TPSSh DFT functional was used for structure optimizations, frequency calculations and relative energy and free energy calculations. Both implicit and explicit solvation models are used to treat the NMP solvent, and some *ab initio* CCSD(T) benchmark calculations were performed in order to check

the accuracy of TPSSh for model reactions involving changes in redox or spin state at nickel centers. A thermodynamic cycle is used to assess the free energy of the steps involving metallic zinc. Full computational details can be found in the SI. The suggested mechanism involves initial reduction of the (phenanthroline)$NiCl_2$ complex **I** by half an equivalent of metallic zinc to yield Ni(I) species **II** and half an equivalent of solvated $ZnCl_2$. (Fig. 7). While the detailed mechanism of this heterogeneous step cannot be described using the quantum-chemical procedure used here, the calculations do enable us to predict the free energy change of this step, which is found to be roughly thermoneutral. On the other hand, subsequent reduction to form a hypothetical (phen)Ni(0) complex (bis-solvated with explicit NMP, **III**) is predicted to be severely endothermic, and presumably thereby not achievable under reaction conditions. Instead, calculations suggest that further reduction of nickel can occur upon binding azobenzene **2** to complex **II** yielding the Ni(I) complex **IV**. Reduction of this with metallic Zn to form the Ni(0) azo **V** is found to be exothermic (by 13.2 kcal mol^{-1}). The change in redox behavior between Ni(I) species **II** and **IV** can be understood by considering the calculated properties of the reduced species **V**. Although this is formally a Ni(0) complex, it involves strong back-donation from Ni as can be seen by considering e.g. the N—N bond length, which is 1.39 Å (compared to 1.26 Å in free **2** and 1.35 Å in **IV**), suggesting donation from the high-energy nickel 3*d* orbitals to the N–N π^* orbital. Note that we do *not* find that this complex has non-innocent Ni(I) character with transfer of one electron to the azo moiety; all attempts to calculate an open-shell singlet state with this bonding pattern revert to the closed-shell singlet described here.

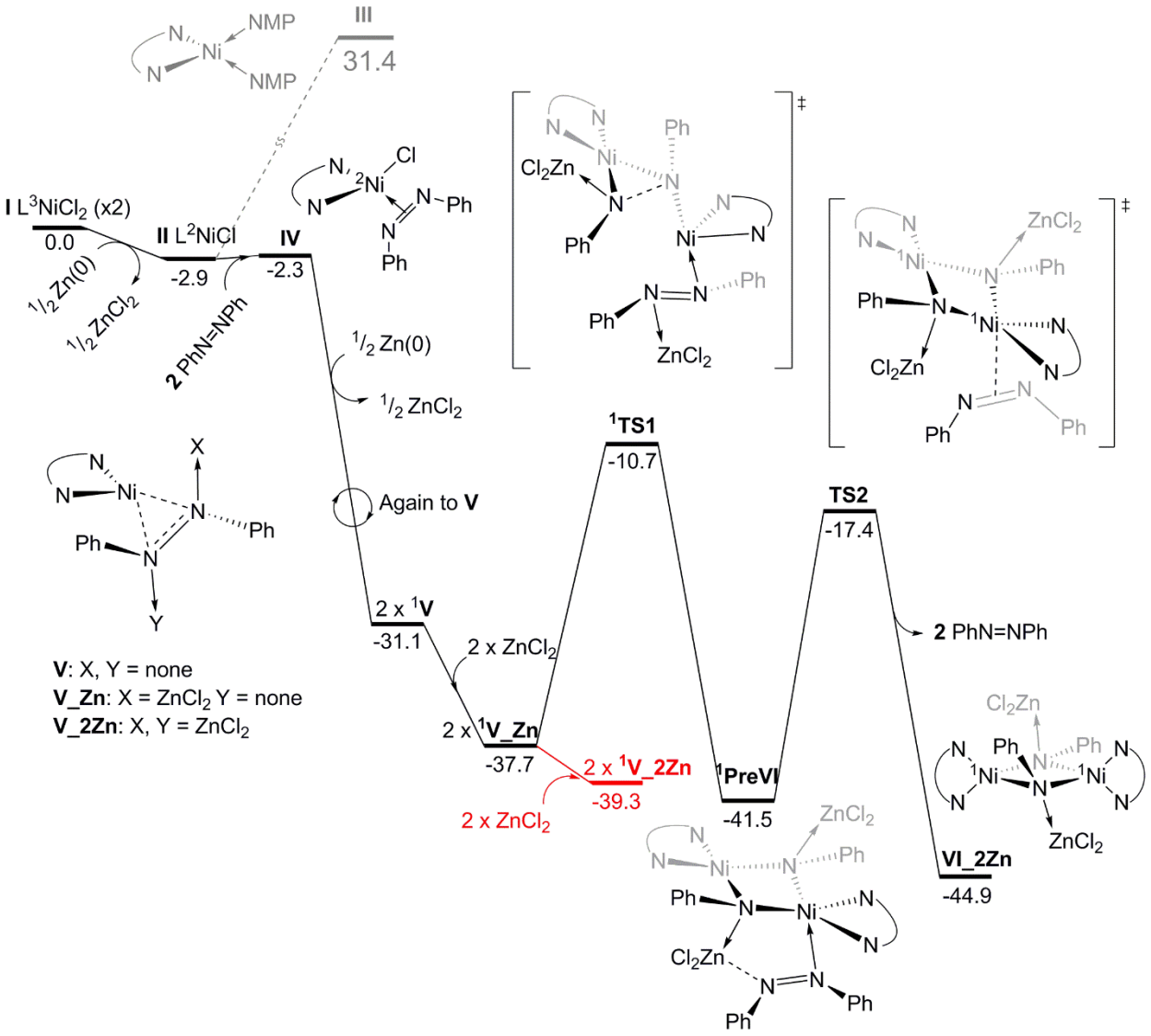

Figure 7. Ni(II) reduction by zinc powder, and possible coordination by $ZnCl_2$ as Lewis acid, and reductive cleavage of diazobenzene; Gibbs free energy values at 363 K in kcal mol^{-1}. Numbers in superscript before compound nomenclature and atoms denote spin pairing at that centre.

Species **V** has quite nucleophilic azo nitrogen atoms, hence it can now coordinate to one or two $ZnCl_2$ metal centres through these nitrogen atoms, thereby generating **V_Zn** or **V_2Zn**. This complexation cannot fully occur in the absence of added $ZnCl_2$, since reduction of the nickel

dichloride generates just one equivalent of $ZnCl_2$ upon forming **V**. Hence the second coordination requires additional $ZnCl_2$. This is shown in Figure 7 by highlighting the second coordination step in red.

The next phase of the mechanism (Fig. 7) leads to breaking of the N=N bond in azobenzene to generate imidonickel(II) complexes such as **VI**, which we predict to be formed in a zinc-coordinating form, **VI_2Zn**. The first step *en route* to **VI_2Zn** from two equivalents of **V_2Zn** is to remove one $ZnCl_2$ from each center, hence starting from **V_Zn**. Two equivalents of **V_Zn** can react through transition state structure **TS1**, with N—N bond splitting in one of the two azo moieties, yielding an analogue of **VI** with a pendant azo moiety, referred to in Figure 7 as **PreVI**. **TS1** lies 27.0 kcal mol^{-1} higher in free energy than two **V_Zn** (or a little bit more relative to two **V_2Zn**). The overall process is almost thermo-neutral, with the product formed after **TS1** (shown in Figure 7 as **PreVI**) lying just 3.8 kcal mol^{-1} lower (in terms of Gibbs free energy) than two **V_Zn** complexes. In order to obtain the Ni-dimer **VI_2Zn** the azo-compound coordinated to one of the Ni centers in **PreVI** needs to be released. This is achieved by crossing **TS2** with a free energy barrier of 24.1 kcal mol^{-1}, with the dimer generated in a very exothermic process from **PreVI**. Overall, the formation of **VI_2Zn** is found to be downhill by 7.2 kcal mol^{-1} from 2 equivalents of **V_Zn**, or by 5.6 kcal mol^{-1} from 2 equivalents of **V_2Zn**. Hence, activation of the N=N bond of the azo to form imido species is predicted to be overall favorable in presence of metallic zinc to generate the required Ni(0) species **V**.

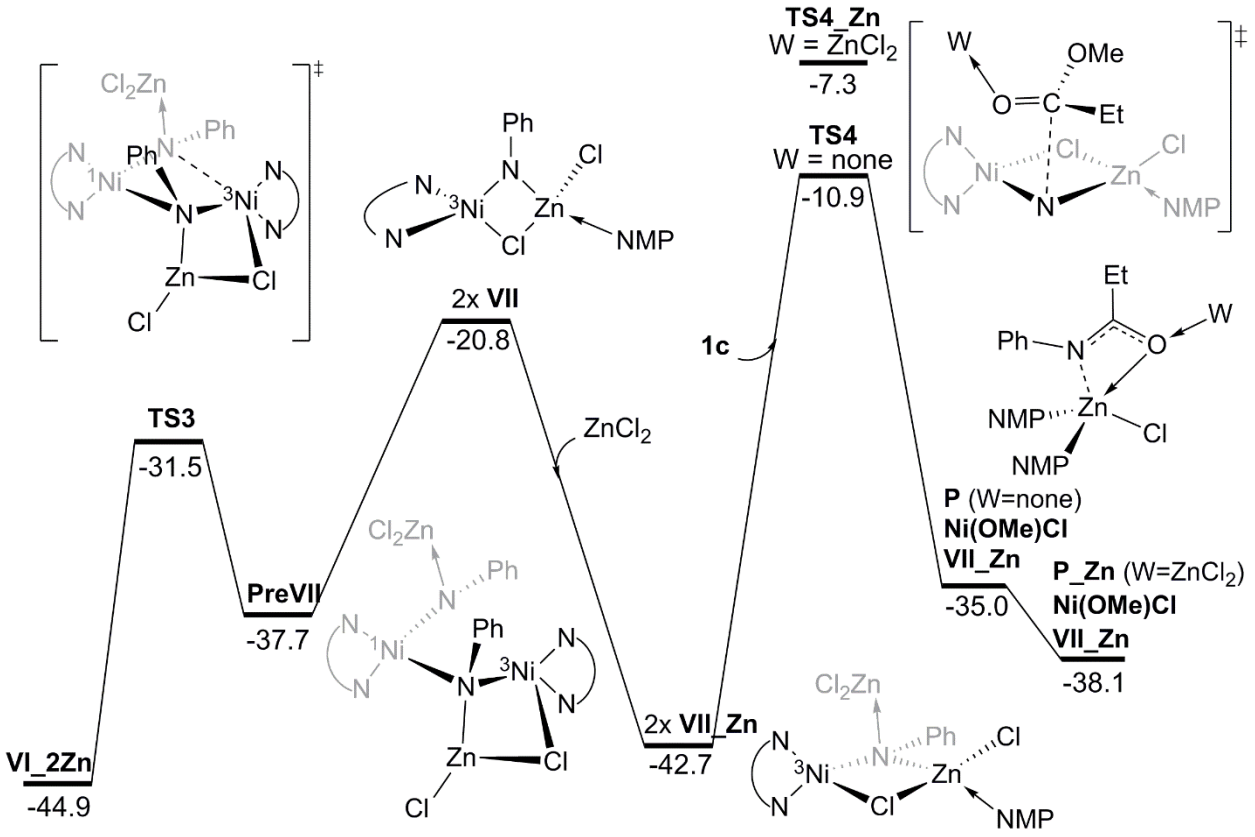

Figure 8. Creation of the NiZn-dimer **VII_Zn** by splitting of the NiNi-dimer **VI_2Zn**, and subsequent nucleophilic addition to the ester **1c**. Gibss free energy values at 363 K in kcal mol^{-1}. Numbers in superscript before atoms denote spin pairing at that centre. **TS4_Zn** is a variant of **TS4** with an additional $ZnCl_2$ but weakened O—Ni interaction.

While species **VI** is a potential nucleophile that could react with the ester **1c**, our calculations (see Supporting Information) show that the combined free energy cost of releasing $ZnCl_2$ and of reaching the barrier is highly unfavorable. On the other hand, we predict that the Ni,Zn-heterodimer **VII_Zn** formed upon splitting **VI_2Zn** into two is a stronger nucleophile. Conversion of the closed shell singlet **VI_2Zn** into two equivalents of **VII_Zn** involves passing through mixed-spin transition state **TS3** in which one of the four Ni-N bonds is being broken, with an

activation free energy of 13.4 kcal mol^{-1}. This leads to formation of complex **PreVII**, which lies 7.2 kcal mol^{-1} higher in free energy than **VI_2Zn**.

In order to obtain two equivalents of the heterodimer **VI_split**, an additional Ni—N bond in **PreVII** needs to break, and an additional Cl—Ni interaction is formed. This splitting process is complex and *a priori* should involve a relatively small barrier above the energy of the two separated fragments **VI_split**, since only relatively simple coordination/decoordination steps are involved. As discussed in the Supporting Information, we suggest that this step does not involve a barrier above the endothermicity. Complexation of **VII** to $ZnCl_2$ then leads to formation of two equivalents of complex **VII_Zn,** lying just 2.2 kcal mol^{-1} higher in free energy compared to the Ni-dimer **VI_2Zn**.

Next, nucleophilic addition of **VII_Zn** to **1a** can lead to the formation of the amide product, with the key step involving **TS4** with an activation barrier of 31.8 kcal mol^{-1} relative to **VII_Zn**, or 34 kcal mol^{-1} relative to **VI_2Zn**. The expected free energy barrier for a process occurring in several hours at 363 K is roughly 28 kcal mol^{-1}, which is consistent with the value of 34 kcal mol^{-1} considering the uncertainties involved in the calculations.[29,30]

3. Discussion

3.1. Reaction sequence. The kinetics measured under high-[$ZnCl_2$] (1st order in Ni and ester and 0th order in azobenzene) could be explained by two scenarios: (i) the ester is activated by the Ni catalyst in the rate determining step, which is followed by reaction with azobenzene. (ii) The azobenzene reagent reacts with the Ni catalyst to form an active nickel species, either irreversibly or in a saturation state, which reacts with the ester in a rate-determining step.

The Hammett study helps to distinguish between the two scenarios. As there is a clear

influence of the electronic properties of the azoarenes on the reaction rate, azobenzene must be activated by nickel prior to the rate determining step.

The kinetics measured under no external $ZnCl_2$ addition (1.5^{th} order in Ni and 0^{th} order in ester and azobenzene) does *not* distinguish the two reaction sequences. However, since the outcome of an ester competition experiment is equal under both conditions (Scheme 2), the intermediate that reacts with ester must be similar, so the reaction sequence must be the same.

3.2. Ni- azobenzene intermediate

For azobenzenes substituted by electron-poor or electron–neutral substituents, the rate of amidation decreases with electron-withdrawing substituents. However, in competition experiments of azobenzenes, the amidation favors azobenzenes with more electron-withdrawing substitutents. The opposite trend observed between the absolute reaction rate and the competition result can be rationalized by the formation and activation of a Ni(0)-azobenzene intermediate before the rate-determining step. This process favors an azobenzene with a more electron-withdrawing substituent. However, the rate-determining step, *i.e.,* the reaction with an ester, is faster for a nickel species derived from an azobenzene with a more electron-donating substituent.

The reaction of a model Ni(0)-azobenzene intermediate with **3F** with ester **1a** in the presence of [$ZnCl_2$] gave the amidation product, supporting the intermediacy of Ni(0)-azobenzene species in the catalysis. The slightly lower yield of the stoichiometric reaction compared to catalysis might originate from unavoidable difference in the employed conditions, even though we tried to mimic the catalytic conditions as much as possible.

Scheme 4. (A) A proposed activation pathway of **3**. (B) Formation of azoarene from nickel(II) imide as reported by Hillhouse

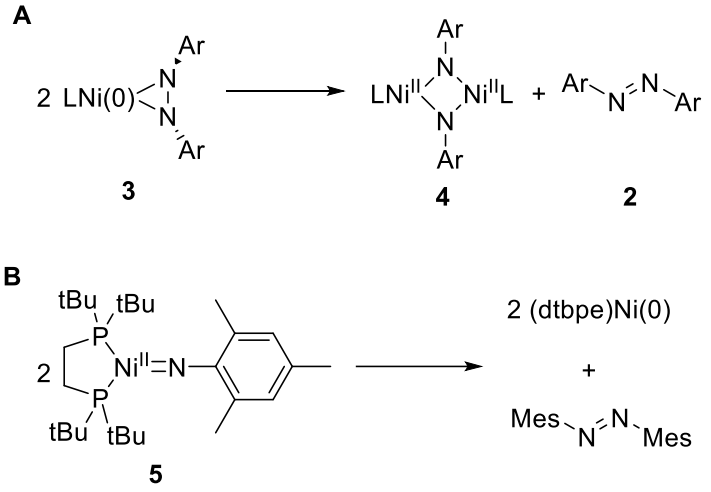

Scheme 4 describes a simplified activation pathway of a Ni(0)-azobenzene intermediate, neglecting the promotion of $ZnCl_2$ for simplicity. Dimerization of two molecules of Ni(0)-azobenzene species (**3**) followed by dissociation of a diazoarene gives a bridging $Ni_2(NAr)_2$ intermediate (**4**) which further reacts with ester to give the amide. Note that in the stoichiometric reaction of $\mathbf{3_F}$ with **1a**, free azoarene $\mathbf{2_F}$ was also obtained as a product, consistent with the proposed pathway. A similar dimerization pathway was proposed by Tonks and co-workers for the formation of a $Ti_2(NAr)_2$ intermediate in the catalytic cycle of pyrrole synthesis from alkynes and azobenzene .[31,32] An analogous reaction was observed between two Ta-azoarene complexes to give two Ta=NAr species.[33] In these reactions the 4-e reductive cleavage of azoarene is balanced by two 2-e oxidations of each metal center. This type of reactivity is also reported for iron,[34] silicium,[35] and aluminium.[36]

For nickel, the cleavage of azobenzene has not been reported to the best of our knowledge,

although Tonks recently reported the N=N cleavage of benzo[c]cinnoline by a Ni_2Ti complex.[37] The reverse reaction, *i.e.* the formation of an azoarene from two Ni=NAr moieties, has been reported by Hillhouse and co-workers: they showed that a diphosphine-ligated terminal nickel imide complex (dtbpe)Ni=NMes (**5**, dtbpe = 1,2-bis-(di-tert-butylphosphino)ethane, Mes = 2,4,6-trimethylaryl) eliminated an azoarene at 80°C (scheme 4B).[38] This example suggests the reverse reaction, the 4-electron reductive cleavage of an azoarene on Ni (as in Scheme 4A), is possible, given the appropriate ligand environment and reaction conditions (e.g., $ZnCl_2$ promotion). DFT computations indicate that when the ligand is phenanthroline, the reaction in Scheme 4A is about 7 kcal mol^{-1} uphill without $ZnCl_2$ (Fig. S23), but in the presence of an $ZnCl_2$, the reaction free energy becomes favorable by 5.6 kcal mol^{-1} (Figure 7). Thus, the corresponding $Ni_2(NAr)_2$ dimer is readily accessible, supported by the recent results obtained by Uyeda and co-workers on the reaction of Ni(bipy)(cod) (cod = cyclooctadiene) with m-terphenylazide.[39]

We attempted to isolate **VI_2Zn** by reacting an azoarene (**2_F**) with phenanthroline and $(DME)NiCl_2$ in the presence of Zn but absence of ester. While a new species could be observed in ^{19}F NMR after the reaction, we were not able to isolate an identifiable compound. Likewise we could not identified a defined complex in the raction of 3_F with $ZnCl_2$. One potential obstacle to isolation and identification may be the relative ease of interconversion of species such as **VI_Zn**, **VI_2Zn** and **VII_2Zn**.

3.3. Influence of $ZnCl_2$. DFT computations show that $ZnCl_2$ can participate in the reactions by (i) stabilizing many intermediates and resting states of the catalyst, such as **V**, **VI**, and **IX** (Fig. 8); (ii) activating the ester by coordinating as a Lewis-acid in some process such as **TS5**; but mostly (iii) by helping the formation of the heterodimer **IX** that is stabilized by 11 kcal mol^{-1} upon

coordination with $ZnCl_2$ **IX_Zn** (see SI); and in turn (iv) stabilizing the Zn-coordinated product **P** that becomes 3.1 kcal mol^{-1} more stable when an extra $ZnCl_2$ coordinates the carboxylic oxygen to yield **P_Zn**. The computational results are consistent with the fact that added $ZnCl_2$ accelerates the reaction and changes the rate order. However, given the wide range of possible $ZnCl_2$ complexes, not all of which could be considered here, the calculations do *not* yield a definitive and quantitative model accounting for all the changes in behavior in the presence of excess zinc chloride. The reaction pathways shown in Figures 7 and 8 should be viewed as limiting cases where the potential roles of $ZnCl_2$ are illustrated.

3.4. Kinetics. DFT computations show that three pathways involving **TS5**, **TS5_Zn**, and **TS4** as the highest point of the energy surface, respectively, can yield the amidation product (Figures 8 and 9). We analyzed the predicted rate orders following these three pathways (SI, kinetic analysis). It was shown that the pathway via **TS5** led to a reaction 2^{nd} order in the concentration of Ni catalyst. The pathway via **TS5_Zn** led to a reaction with a non-linear dependence on [azobenzene]. These rate orders contradicted the experimental findings.

On the other hand, the suggested and preferred pathway via **TS4** led to a reaction with rate orders that agreed with the experimental values. At a low [$ZnCl_2$], the reaction would be 0^{th} order in both [azobenzene] and [ester], and $1+\alpha$ ($0 < \alpha < 1$) order in [Ni]. At high [$ZnCl_2$], the reaction would be 1^{st} order in [Ni] and [ester], and 0^{th} order in [azobenzene]. Therefore, the computed lowest-energy reaction pathway, with significant involvement of $ZnCl_2$, is consistent with the kinetic data.

3.5. Catalytic cycle. The complexity of the catalytic system hinders a decisive determination of

the full catalytic cycle: compared to the vast amount of potential intermediate species, we have only managed to consider a limited number. Nonetheless, the kinetic experiments and calculations on key intermediates have provided valuable insights. Based on these, we propose the catalytic cycle depicted in Scheme 5. Nickel(II) (**I**, X = Cl or X = OMe) is readily reduced to Ni(I) (**II**) by Zn. **II** can bind an azoarene, forming complex **IV**. While the adduct formation is uphill, it allows for facile reduction to Ni(0) azo adduct **V**, which readily binds a zinc salt to form **V_Zn**. Subsequently, two molecules of **V_Zn** combine to form dinickel bisimide **VI_2Zn**, releasing one equivalent of azoarene. **VI_2Zn** is in equilibrium with other Ni/Zn complexes **VI_Zn**, **VII** and **VII_Zn**, via the breaking up of dimers to monomers (**VI_2Zn** to **VII**) and the exchange of weakly binding zinc salts (**VI_2Zn** to **VI_Zn** and **VII** to **VII_Zn**). This equilibrating mixture is pushed forward by reaction of **VII_Zn** with an ester, forming a zinc complex of the product amide and regenerating **I**.

As mentioned above, a wide range of $ZnCl_2$ complexes might exist in the reaction medium. Species **VI_2Zn** and its behavior should be viewed as a limiting and exemplifying case of possible mechanisms.

Scheme 5. Tentative catalytic cycle for the amidation of ester **1** with azoarene **2**.

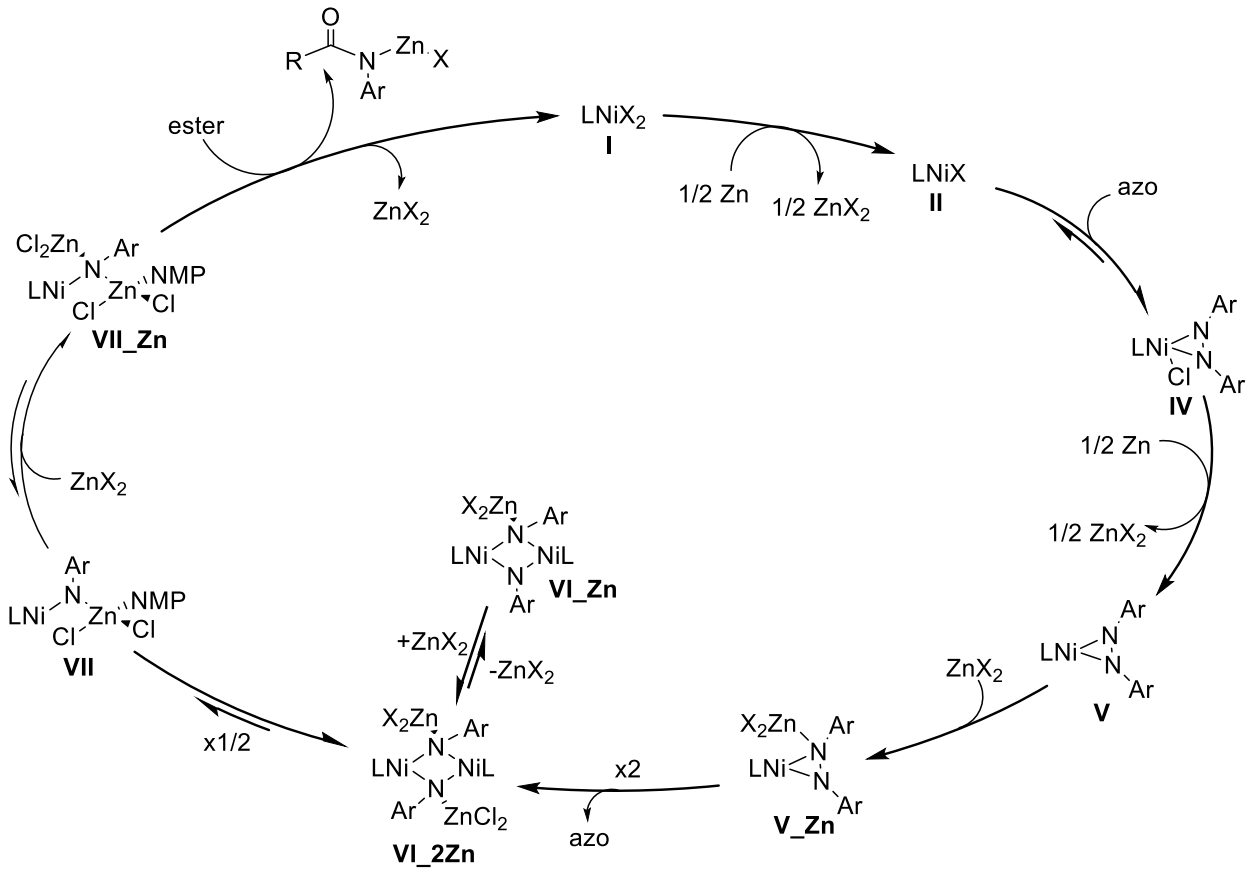

4. Conclusion

In summary, our combined experimental and theoretical study of the recently developed Ni-catalyzed reductive amidation of esters has revealed an intricate mechanism. Azobenzene is identified as the terminal nitrogen intermediate from reduction of nitrobenzene. An azobenzene is then activated by a nickel catalyst, via a Ni(0)-azobenzene intermediate, before reacting with an ester to give the amide. A Hammett study reveals that the activation of azobenzene is irreversible and occurs before the rate determining step. $ZnCl_2$ has a strong influence on both reaction rates and orders. DFT computations suggest several possible roles of $ZnCl_2$ such as stabilization of intermediates and activation of ester. Based on DFT computations and kinetics, we propose that azobenzene is activated, by a 4-eletron reductive cleavage on two Ni(0) centers, to give a bridging $Ni_2(imide)_2$ intermediate. $ZnCl_2$ promotes this activation by coordination to the Ni species as well

as by forming a heterobimetallic bridging imide. The latter reacts in a rate-determining step with ester to complete the amidation. We are currently seeking to intercept the imide intermediates with other reaction partners so that new synthetic methods can be developed using stable and easily accessible azoarenes as a nitrogen source.

AUTHOR INFORMATION

Corresponding Author

Jeremy Harvey, jeremy.harvey@kuleuven.be; Xile Hu, xile.hu@epfl.ch

Author Contributions

Marten L. Ploeger and Andrea Darù contributed equally to this work. All authors have given approval to the final version of the manuscript. The authors declare no competing financial interests.

ASSOCIATED CONTENT

Supporting Information. The following files are available free of charge.

Experimental details, additional IR and NMR data, kinetic analysis, and further computational details (pdf).

ACKNOWLEDGMENT

This work is funded by the European Union's Horizon 2020 research and innovation programme under the Marie Curie Skłodowska–Curie grant agreement. Project ID: 675020. Project name: Non-Noble Metal Catalysis - NoNoMeCat. The computational resources and services used in this

work were provided by the VSC (Flemish Supercomputer Center), funded by the Research Foundation Flanders (FWO) and the Flemish Government – department EWI.

REFERENCES

(1) Ono, N. *The Nitro Group in Organic Synthesis*; Wiley-VCH: New York, 2001; pp 302-321.
(2) Booth, G. Nitro Compounds, Aromatic. In *Ullmann's Encyclopedia of Industrial Chemistry*; Wiley-VCH: New York, 2012; pp 301-349.
(3) Yadav, M. R.; Nagaoka, M.; Kashihara, M.; Zhong, R.-L.; Miyazaki, T.; Sakaki, S.; Nakao, Y. The Suzuki–Miyaura Coupling of Nitroarenes. *Journal of the American Chemical Society* **2017**, *139* (28), 9423–9426. https://doi.org/10.1021/jacs.7b03159.
(4) Beck, J. R. Nucleophilic Displacement of Aromatic Nitro Groups. *Tetrahedron* **1978**, *34* (14), 2057–2068. https://doi.org/10.1016/0040-4020(78)89004-8.
(5) Zhang, J.; Chen, J.; Liu, M.; Zheng, X.; Ding, J.; Wu, H. Ligand-Free Copper-Catalyzed Coupling of Nitroarenes with Arylboronic Acids. *Green Chemistry* **2012**, *14* (4), 912. https://doi.org/10.1039/c2gc16539b.
(6) Zheng, X.; Ding, J.; Chen, J.; Gao, W.; Liu, M.; Wu, H. The Coupling of Arylboronic Acids with Nitroarenes Catalyzed by Rhodium. *Organic Letters* **2011**, *13* (7), 1726–1729. https://doi.org/10.1021/ol200251x.
(7) Bahekar, S. S.; Sarkate, A. P.; Wadhai, V. M.; Wakte, P. S.; Shinde, D. B. CuI Catalyzed CS Bond Formation by Using Nitroarenes. *Catalysis Communications* **2013**, *41*, 123–125. https://doi.org/10.1016/j.catcom.2013.07.019.
(8) Tong, S.; Xu, Z.; Mamboury, M.; Wang, Q.; Zhu, J. Aqueous Titanium Trichloride Promoted Reductive Cyclization of *o* -Nitrostyrenes to Indoles: Development and Application to the Synthesis of Rizatriptan and Aspidospermidine. *Angewandte Chemie International Edition* **2015**, *54* (40), 11809–11812. https://doi.org/10.1002/anie.201505713.
(9) Gui, J.; Pan, C.-M.; Jin, Y.; Qin, T.; Lo, J. C.; Lee, B. J.; Spergel, S. H.; Mertzman, M. E.; Pitts, W. J.; La Cruz, T. E.; Schmidt, M. A.; Darvatkar, N.; Natarajan, S. R.; Baran, P. S. Practical Olefin Hydroamination with Nitroarenes. *Science* **2015**, *348* (6237), 886–891. https://doi.org/10.1126/science.aab0245.
(10) Rauser, M.; Ascheberg, C.; Niggemann, M. Electrophilic Amination with Nitroarenes. *Angewandte Chemie International Edition* **2017**, *56* (38), 11570–11574. https://doi.org/10.1002/anie.201705356.
(11) Zhu, K.; Shaver, M. P.; Thomas, S. P. Chemoselective Nitro Reduction and Hydroamination Using a Single Iron Catalyst. *Chemical Science* **2016**, *7* (5), 3031–3035. https://doi.org/10.1039/C5SC04471E.
(12) Cheung, C. W.; Shen, N.; Wang, S.-P.; Ullah, A.; Hu, X.; Ma, J.-A. Manganese-Mediated Reductive Amidation of Esters with Nitroarenes. *Organic Chemistry Frontiers* **2019**, *6* (6), 756-761. https://doi.org/10.1039/C8QO01405A.
(13) Cheung, C. W.; Ma, J.-A.; Hu, X. Manganese-Mediated Reductive Transamidation of Tertiary Amides with Nitroarenes. *Journal of the American Chemical Society* **2018**, *140* (22), 6789–6792. https://doi.org/10.1021/jacs.8b03739.

(14) Cheung, C. W.; Hu, X. Amine Synthesis via Iron-Catalysed Reductive Coupling of Nitroarenes with Alkyl Halides. *Nature Communications* **2016**, *7* (1). https://doi.org/10.1038/ncomms12494.
(15) Cheung, C. W.; Leendert Ploeger, M.; Hu, X. Amide Synthesis *via* Nickel-Catalysed Reductive Aminocarbonylation of Aryl Halides with Nitroarenes. *Chemical Science* **2018**, *9* (3), 655–659. https://doi.org/10.1039/C7SC03950F.
(16) Cheung, C. W.; Ploeger, M. L.; Hu, X. Direct Amidation of Esters with Nitroarenes. *Nature Communications* **2017**, *8*, 14878. https://doi.org/10.1038/ncomms14878.
(17) Cheung, C. W.; Ploeger, M. L.; Hu, X. Nickel-Catalyzed Reductive Transamidation of Secondary Amides with Nitroarenes. *ACS Catalysis* **2017**, *7* (10), 7092–7096. https://doi.org/10.1021/acscatal.7b02859.
(18) Mahata, A.; Rai, R. K.; Choudhuri, I.; Singh, S. K.; Pathak, B. Direct vs. Indirect Pathway for Nitrobenzene Reduction Reaction on a Ni Catalyst Surface: A Density Functional Study. *Phys. Chem. Chem. Phys.* **2014**, *16* (47), 26365–26374. https://doi.org/10.1039/C4CP04355C.
(19) Guan, B.-T.; Wang, Y.; Li, B.-J.; Yu, D.-G.; Shi, Z.-J. Biaryl Construction via Ni-Catalyzed C−O Activation of Phenolic Carboxylates. *Journal of the American Chemical Society* **2008**, *130* (44), 14468–14470. https://doi.org/10.1021/ja8056503.
(20) Hie, L.; Fine Nathel, N. F.; Hong, X.; Yang, Y.-F.; Houk, K. N.; Garg, N. K. Nickel-Catalyzed Activation of Acyl C−O Bonds of Methyl Esters. *Angewandte Chemie International Edition* **2016**, *55* (8), 2810–2814. https://doi.org/10.1002/anie.201511486.
(21) Burés, J. A Simple Graphical Method to Determine the Order in Catalyst. *Angewandte Chemie International Edition* **2016**, *55* (6), 2028–2031. https://doi.org/10.1002/anie.201508983.
(22) Burés, J. Variable Time Normalization Analysis: General Graphical Elucidation of Reaction Orders from Concentration Profiles. *Angewandte Chemie International Edition* **2016**, *55* (52), 16084–16087. https://doi.org/10.1002/anie.201609757.
(23) Schmidt, A. F.; Kurokhtina, A. A.; Larina, E. V. Differential Selectivity Measurements and Competitive Reaction Methods as Effective Means for Mechanistic Studies of Complex Catalytic Reactions. *Catal. Sci. Technol.* **2014**, *4* (10), 3439–3457. https://doi.org/10.1039/C4CY00479E.
(24) Otsuka, S.; Yoshida, T.; Tatsuno, Y. Isocyanide-Nickel(0) and -Palladium(0) Complexes Involving Unsaturated Ligands. *Journal of the American Chemical Society* **1971**, *93* (24), 6462–6469. https://doi.org/10.1021/ja00753a021.
(25) Muetterties, E. L.; Pretzer, W. R.; Thomas, M. G.; Beier, B. F.; Thorn, D. L.; Day, V. W.; Anderson, A. B. Metal Clusters in Catalysis. 14. The Chemistry of Dinuclear Metal-Acetylene Complexes. *Journal of the American Chemical Society* **1978**, *100* (7), 2090–2096. https://doi.org/10.1021/ja00475a019.
(26) Link, H.; Reiss, P.; Chitsaz, S.; Pfistner, H.; Fenske, D. Synthese Und Molekülstrukturen von Amido- Und Imidoverbrückten Clustern Elektronenreicher Übergangsmetalle. *Zeitschrift für anorganische und allgemeine Chemie* **2003**, *629* (5), 755–768. https://doi.org/10.1002/zaac.200390138.
(27) Zurita, D. A.; Flores-Alamo, M.; García, J. J. Catalytic Transfer Hydrogenation of Azobenzene by Low-Valent Nickel Complexes: A Route to 1,2-Disubstituted Benzimidazoles and 2,4,5-Trisubstituted Imidazolines. *Dalton Transactions* **2016**, *45* (25), 10389–10401. https://doi.org/10.1039/C6DT01674J.

(28) Dinjus, E.; Gorski, I.; Matschiner, H.; Uhlig, E.; Walther, D. Substitutionsreaktionen mit Gemischtligand-Komplexen des Nickel(0). I. Reaktionen mit Heteroolefinen. *Zeitschrift f*[illegible]*r anorganische und allgemeine Chemie* **1977**, *436* (1), 39–46. https://doi.org/10.1002/zaac.19774360104.

(29) Liu, Z.; Patel, C.; Harvey, J. N.; Sunoj, R. B. Mechanism and Reactivity in the Morita–Baylis–Hillman Reaction: The Challenge of Accurate Computations. *Physical Chemistry Chemical Physics* **2017**, *19* (45), 30647–30657. https://doi.org/10.1039/C7CP06508F.

(30) Harvey, J. N.; Himo, F.; Maseras, F.; Perrin, L. Scope and Challenge of Computational Methods for Studying Mechanism and Reactivity in Homogeneous Catalysis. *ACS Catalysis* **2019**, *9* (8), 6803–6813. https://doi.org/10.1021/acscatal.9b01537.

(31) Gilbert, Z. W.; Hue, R. J.; Tonks, I. A. Catalytic Formal [2+2+1] Synthesis of Pyrroles from Alkynes and Diazenes via TiII/TiIV Redox Catalysis. *Nature Chemistry* **2016**, *8* (1), 63–68. https://doi.org/10.1038/nchem.2386.

(32) Davis-Gilbert, Z. W.; Wen, X.; Goodpaster, J. D.; Tonks, I. A. Mechanism of Ti-Catalyzed Oxidative Nitrene Transfer in [2 + 2 + 1] Pyrrole Synthesis from Alkynes and Azobenzene. *Journal of the American Chemical Society* **2018**, *140* (23), 7267–7281. https://doi.org/10.1021/jacs.8b03546.

(33) Aubart, M. A.; Bergman, R. G. Tantalum-Mediated Cleavage of an NN Bond in an Organic Diazene (Azoarene) to Produce an Imidometal (MNR) Complex: An η^2-Diazene Complex Is Not an Intermediate. *Organometallics* **1999**, *18* (5), 811–813. https://doi.org/10.1021/om9809668.

(34) Bellows, S. M.; Arnet, N. A.; Gurubasavaraj, P. M.; Brennessel, W. W.; Bill, E.; Cundari, T. R.; Holland, P. L. The Mechanism of N–N Double Bond Cleavage by an Iron(II) Hydride Complex. *Journal of the American Chemical Society* **2016**, *138* (37), 12112–12123. https://doi.org/10.1021/jacs.6b04654.

(35) Takeuchi, K.; Ichinohe, M.; Sekiguchi, A. Access to a Stable Si_2N_2 Four-Membered Ring with Non-Kekulé Singlet Biradical Character from a Disilyne. *Journal of the American Chemical Society* **2011**, *133* (32), 12478–12481. https://doi.org/10.1021/ja2059846.

(36) Zhao, Y.; Liu, Y.; Yang, L.; Yu, J.-G.; Li, S.; Wu, B.; Yang, X.-J. Mechanistic Insight into the N□N Bond-Cleavage of Azo-Compounds That Was Induced by an Al□Al-Bonded Compound [L2−AlII□AlIIIL2−]. *Chemistry - A European Journal* **2012**, *18* (19), 6022–6030. https://doi.org/10.1002/chem.201103607.

(37) Dunn, P. L.; Chatterjee, S.; MacMillan, S. N.; Pearce, A. J.; Lancaster, K. M.; Tonks, I. A. The 4-Electron Cleavage of a N═N Double Bond by a Trimetallic $TiNi_2$ Complex. *Inorganic Chemistry* **2019**, *58* (17), 11762–11772. https://doi.org/10.1021/acs.inorgchem.9b01805.

(38) Mindiola, D. J.; Waterman, R.; Iluc, V. M.; Cundari, T. R.; Hillhouse, G. L. Carbon–Hydrogen Bond Activation, C–N Bond Coupling, and Cycloaddition Reactivity of a Three-Coordinate Nickel Complex Featuring a Terminal Imido Ligand. *Inorganic Chemistry* **2014**, *53* (24), 13227–13238. https://doi.org/10.1021/ic5026153.

(39) Powers, I. G.; Kiattisewee, C.; Mullane, K. C.; Schelter, E. J.; Uyeda, C. A 1,2-Addition Pathway for $C(Sp_2)$−H Activation at a Dinickel Imide. *Chemistry - A European Journal* **2017**, *23* (32), 7694–7697. https://doi.org/10.1002/chem.201701855.

TOC Graphic

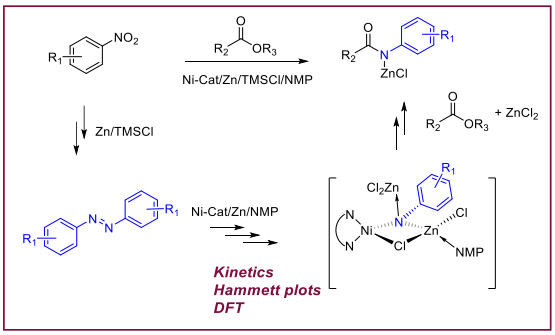
NO2
R1
R2
OR3
Ni-Cat/Zn/TMSCl/NMP
O
N
ZnCl
Zn/TMSCl
+ ZnCl2
Ni-Cat/Zn/NMP
Cl2Zn
Ni
Zn
Cl
NMP
Kinetics
Hammett plots
DFT